Inorg. Chem. **2002**, *41*, 4664–4672

Flux Growth of Vanadyl Pyrophosphate, $(VO)_2P_2O_7$, and Spin Dimer Analysis of the Spin Exchange Interactions of $(VO)_2P_2O_7$ and Vanadyl Hydrogen Phosphate, $VO(HPO_4)\cdot 0.5H_2O$

Hyun-Joo Koo and Myung-Hwan Whangbo*

Department of Chemistry, North Carolina State University, Raleigh, North Carolina 27695-8204

Paul D. VerNooy,* Charlie C. Torardi, and William J. Marshall

Central Research and Development, DuPont Company, Experimental Station, Wilmington, Delaware 19880-0262

Received April 1, 2002

Large transparent blue crystals of vanadyl pyrophosphate, $(VO)_2P_2O_7$, were grown from a phosphorus pentoxide flux, and the single-crystal X-ray structure of $(VO)_2P_2O_7$ was determined with high precision. On the basis of spin dimer analysis, we examined the spin exchange interactions of $(VO)_2P_2O_7$ and its precursor $VO(HPO_4)\cdot 0.5H_2O$. Our analysis of $(VO)_2P_2O_7$ using two high-precision crystal structures shows unambiguously that the V3–V4 chain has a larger spin gap than does the V1–V2 chain and that the super-superexchange (V–O···O–V) interaction is stronger than the superexchange (V–O–V) interaction in the V3–V4 chain while the opposite is true in the V1–V2 chain. Our analysis of $VO(HPO_4)\cdot 0.5H_2O$ reveals that the superexchange interaction must dominate over the super-superexchange interaction, in disagreement with the conclusion from a powder neutron scattering study of $VO(DPO_4)\cdot 0.5D_2O$.

1. Introduction

Vanadyl pyrophosphate (VPO), $(VO)_2P_2O_7$, has been the focus of intense interest over the past 30 years largely because it is an efficient catalyst for oxidizing *n*-butane to maleic anhydride, an important commercial intermediate.[1−4] These studies have been limited to either microcrystalline powders or disordered crystals due to the fact that the growth of high-quality crystals has been elusive. The favored synthetic route to $(VO)_2P_2O_7$ involves decomposition of its precursor vanadyl hydrogen phosphate (VHP), $VO(HPO_4)\cdot 0.5H_2O$.[5,6] Although the dehydration of VHP to VPO is topotactic,[5−9] considerable disorder can arise during the condensation of the phosphate groups to pyrophosphates and the linking of the layers into a three-dimensional structure. Other roadblocks have been the need to maintain the oxidation state of vanadium at +4 and the difficulty in finding a nonreactive molten salt flux. Consequently, in the most reported crystal structures of VPO, the accuracy of the atomic coordinates is quite low.[10] Only very recently, a single-crystal structure of VPO with high precision was reported by Geupel et al.,[11] who prepared high-quality single-crystal samples by melt-pulling.

The recent interest in VPO has been in the area of its magnetic properties. The magnetic susceptibility of VPO was found well described by the spin-1/2 alternating antiferromagnetic chain model[12] and subsequently by the spin ladder model.[13,14] However, later studies showed conclusively[15,16]

* To whom correspondence should be addressed. E-mail (M.-H.W.): mike_whangbo@ncsu.edu.

(1) Bergman, R. I.; Frisch, N. W. U.S. Patent 3,293,268, 1966.
(2) Bordes, E.; Courtine, P. *J. Chem. Soc., Chem. Commun*. **1985**, 294.
(3) Contractor, R. M.; Bergna, H. E.; Horowitz, H. S.; Blackstone, C. M.; Malone, B.; Torardi, C. C.; Griffiths, B.; Chowdhry, U.; Sleight, A. W. *Catal. Today* **1987**, *1*, 49.
(4) Centi, G.; Trifirò, F. *Chem. Eng. Sci*. **1990**, *45*, 2589.
(5) Torardi, C. C.; Calabrese, J. C. *Inorg. Chem*. **1984**, *23*, 1308.
(6) Leonowicz, M. E.; Johnson, J. W.; Brody, J. F.; Shannon, H. F., Jr.; Newsam, J. M. *J. Solid State Chem*. **1985**, *56*, 370.
(7) Bordes, E.; Courtine, P.; Johnson, J. W. *J. Solid State Chem.* **1984**, *55*, 270.
(8) Johnson, J. W.; Johnston, D. C.; Jacobson, A. J.; Brody, J. F. *J. Am. Chem. Soc*. **1984**, *106*, 8123.
(9) Torardi, C. C.; Li, Z. G.; Horowitz, H. S.; Liang, W.; Whangbo, M.-H. *J. Solid State Chem*. **1995**, *119*, 349.
(10) Hiroi, Z.; Azuma, M.; Fujishiro, Y.; Saito, T.; Takano, M.; Izumi, F.; Kamiyama, T.; Ikeda, T. *J. Solid State Chem*. **1999**, *146*, 369 and the references therein.
(11) Geupel, S.; Pilz, K.; van Smaalen, S.; Büllesfeld, F.; Prokofiev, A.; Assmus, W. *Acta Crystallogr., Sect. C* **2002**, *58*, i9.

10.1021/ic020249c CCC: $22.00
Published on Web 08/14/2002

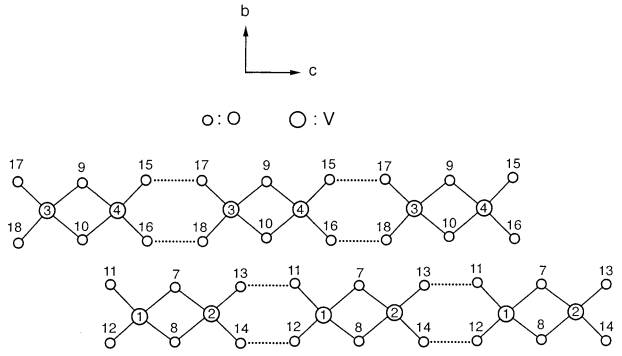

Figure 1. Arrangements of the V and O atoms in the V1−V2 and V3−V4 ribbon chains in the ambient pressure orthorhombic structures of $(VO)_2P_2O_7$.

that the spin-1/2 alternating antiferromagnetic chain model is correct for VPO. The structural building blocks of VPO are V_2O_8 dimers and pyrophosphates, P_2O_7. Each V_2O_8 dimer is obtained from two VO_5 square pyramids by sharing an O−O edge of their basal planes, and each P_2O_7 unit from two PO_4 tetrahedra by sharing an oxygen corner. The structural feature leading to the spin-1/2 alternating antiferromagnetic chain model for VPO is the "ribbon chains" along the crystallographic *c*-direction (Figures 1 and 2),[10,15,16] in which adjacent V_2O_8 dimers are linked by two O−P−O bridges such that the basal planes of the dimers form ribbons. Along each ribbon-chain, the superexchange (SE) interactions, which occur through the V−O−V linkages within each V_2O_8 dimer, alternate with the super-superexchange (SSE) interactions, which occur through the V−O···O−V linkages between adjacent V_2O_8 dimers. Since the SE and SSE antiferromagnetic interactions differ in strength, a spin gap results. The ambient pressure orthorhombic (APO) structure of VPO has two spin gaps,[16,17] because it has two structurally different ribbon chains.[11] The high-pressure orthorhombic (HPO) structure of VPO has a single spin gap, and it consists of identical ribbon chains.[18,19] The VHP phase also consists of ribbon chains (Figure 3) so that there are both SE and SSE interactions to consider in each ribbon chain. However, the magnetic susceptibility measurements[8] of VHP and the neutron scattering measurements of its deuterium analogue, $VO(DPO_4)\cdot 0.5D_2O$ (hereafter referred to as VDP),[20] indicated that the magnetic structures of VHP and VDP are well described by the isolated dimer model.

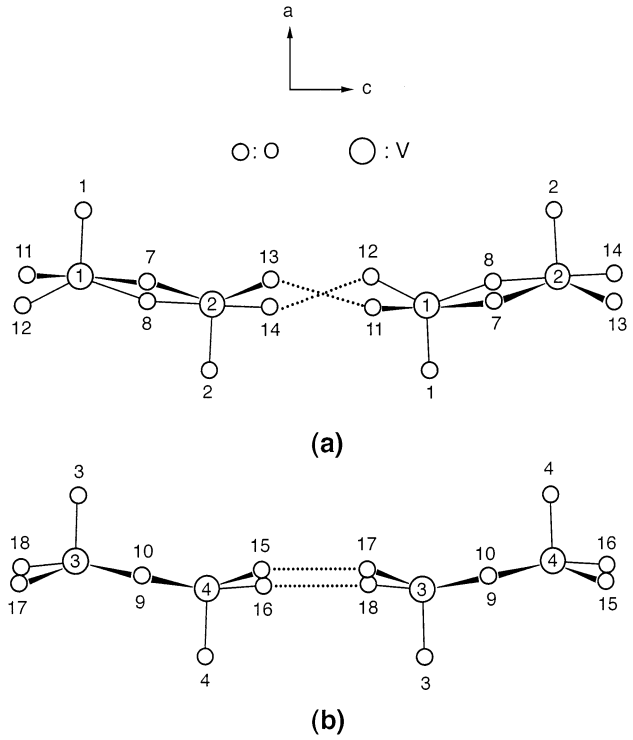

Figure 2. Perspective views along the *b*-direction of the (a) V1−V2 and (b) V3−V4 ribbon chains in the ambient pressure orthorhombic structures of $(VO)_2P_2O_7$.

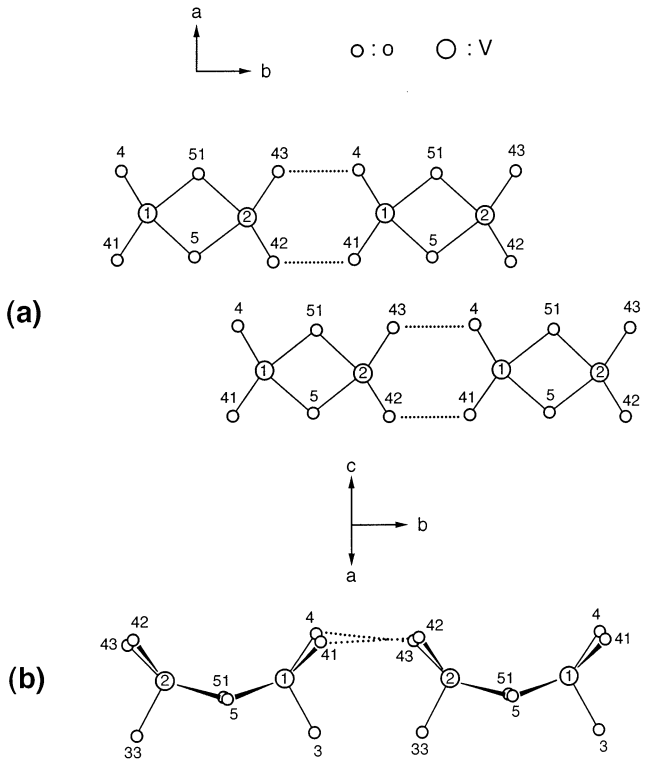

Figure 3. (a) Arrangements of the V and O atoms in the ribbon chains of $VO(HPO_4)\cdot 0.5H_2O$. (b) Perspective view of the ribbon chains of $VO(HPO_4)\cdot 0.5H_2O$.

The spin exchange interactions of VPO were recently examined[21] from the viewpoint of the electronic structures

(12) Johnston, D. C.; Johnson, J. W.; Goshorn, D. P.; Jacobson, A. J. *Phys. Rev. B* **1987**, *35*, 219.
(13) Barnes, T.; Riera, J. *Phys. Rev. B* **1994**, *50*, 6817.
(14) Eccleston, R. S.; Barnes, T.; Brody, J.; Johnson, J. W. *Phys. Rev. Lett.* **1994**, *73*, 2626.
(15) Garret, A. W.; Nagler, S. E.; Tennant, D. A.; Sales, B. C.; Barnes, T. *Phys. Rev. Lett.* **1997**, *79*, 745.
(16) Kikuchi, J.; Motoya, K.; Yamauchi, T.; Ueda, Y. *Phys. Rev. B* **1999**, *60*, 6731.
(17) Johnston, D. C.; Saito, T.; Azuma, M.; Takano, M.; Yamauchi, T.; Ueda, Y. *Phys. Rev. B* **2001**, *64*, 134403.
(18) Azuma, M.; Saito, T.; Fujishiro, Y.; Hiroi, Z.; Takano, M.; Izumi, F.; Kamiyama, T.; Ikeda, T.; Narumi, Y.; Kindo, K. *Phys. Rev. B* **1999**, *60*, 10145.
(19) Saito, T.; Terashima, T.; Azuma, M.; Takano, M.; Goto, T.; Ohta, H.; Utsumi, W.; Bordet, P.; Johnston, D. C. *J. Solid State Chem.* **2000**, *153*, 124.
(20) Tennant, D. A.; Nagler, S. E.; Garrett, A. W.; Barnes, T.; Torardi, C. C. *Phys. Rev. Lett.* **1997**, *78*, 4998.
(21) Koo, H.-J.; Whangbo, M.-H. *Inorg. Chem.* **2000**, *39*, 3599.

of their spin dimers (i.e., structural units containing two adjacent spins). By considering the nodal properties of the magnetic orbitals of the VO_5 square pyramids, this study showed why the spin exchange interaction along the *a*-direction (i.e., the ladder direction) should be weakly ferromagnetic rather than antiferromagnetic and also why the SSE interactions between adjacent ribbon chains in the *bc*-plane should be significantly weaker than those within each ribbon-chain. Due to the low accuracy of the APO crystal structures of VPO available at the time, however, this study was unable to conclude unambiguously which ribbon-chain (V1−V2 or V3−V4) has a larger spin gap and which spin exchange interaction (SE or SSE) is stronger in each ribbon-chain. In this work we attempt to answer these questions unambiguously by performing spin dimer analysis for two high-quality crystal structures now available (i.e., Geupel et al.'s[11] and our own to be described below). The success of the isolated dimer model for the VHP phase implies that either the SE or the SSE interaction is strongly reduced. Consideration of orbital overlaps by Beltrán-Porter et al. suggested that the SE interaction probably dominates over the SSE interaction in VHP,[22] but the neutron scattering study[20] of VDP reached the opposite conclusion. Thus, we will examine the spin exchange interactions of VHP by spin dimer analysis in an attempt to gain insight into the origin of this discrepancy between theory and experiment.

This work is organized as follows: Section 2 describes the preparation of large fully ordered single-crystal samples of VPO by the flux growth method and the determination of the crystal structure by single-crystal X-ray diffraction. Section 3 compares the geometrical parameters of the ribbon chains found in the VPO and VHP phases. Section 4 describes the essence of spin dimer analysis. We analyze the spin exchange interactions of VPO in section 5 and then assign the experimentally deduced spin exchange parameters. The spin exchange interactions of the VHP phase are discussed in section 6. Important conclusions of our work are summarized in section 7.

2. Synthesis and Structure Determination of the VPO Phase

The present synthesis employed phosphorus pentoxide (P_2O_5) as a reactive flux. The system was anhydrous and free of impurities that could lead to other products. By necessity, the reaction was run in a sealed gold tube under pressure, which prevented loss of oxygen and maintained the V^{4+} oxidation state.

A 1.0 g sample of VO_2 (Johnson-Matthey) and 3.64 g of P_2O_5 (Baker) were placed, without premixing, into a 3/8 in. gold tube (0.010 in. wall). Except for working quickly, no special precautions were taken to prevent moisture absorption by the P_2O_5. After being welded shut with a propane/oxygen torch, the tube was subjected to ~3 kbar isostatic pressure of argon and heated 10°/min to 900 °C, held at 900 °C for 10 h, and cooled slowly to 700 °C over 36 h. The furnace was then shut off and cooled to room temperature over several minutes. The excess flux was dissolved in water, leaving transparent, blue, blocky crystals of VPO and black crystals of $V_4(P_2O_7)_3$.[23] The largest crystals of VPO were about 4 mm in length. Alternatively, the gold tube could be crimped shut and sealed in an evacuated quartz tube to allow heating in a conventional furnace, but this method yielded fewer and smaller crystals. Minor variations in the synthesis conditions will lead to the crystallization of other blue phases. $VO(PO_3)_2$[24] is formed if a slower cooling rate is used, and $VO(H_2PO_4)_2$[25] is formed if sufficient water is present.

Many colors of VPO crystals have been reported over the years, but blue has not been among them. Inorganic V^{4+} compounds such as those mentioned above and vanadyl sulfate are typically blue. Other oxidation states generally give green, yellow, or black compounds. The color of the VPO samples prepared by the melt-pulling method was reported to be dark-green.[11] The pure blue color of our crystal samples is strong evidence that the samples consist of V^{4+} ions and are not contaminated by V^{5+} ions. This is supported by the crystal structure, which shows no vacancies or disorder.

P_2O_5 is an unusual flux in that, at atmospheric pressure, it sublimes before it melts. It also occurs in several modifications, each with its own vapor pressure and melting point.[26] The phase with the highest vapor pressure, ~6 atm, is also the major constituent of commercial P_2O_5. However, this modification slowly transforms above about 400 °C to phases with lower vapor pressures. Nevertheless, external pressure on the gold tube is necessary to prevent its rupturing.

Our single-crystal X-ray diffraction study[27] on a small, uncut crystal of VPO leads to the following results: $a = 7.729(1)$, $b = 9.583(1)$, $c = 16.581(2)$ Å; $V = 1228.1(3)$ Å^3; fw = 307.8; $Z = 8$. The positional parameters are summarized in Table 1.[28] Intensity control reflections were scanned every 90 min of exposure time. No decay was observed.

The systematic absences were consistent with the space groups $Pca2_1$ (No. 29) and *Pcam* (No. 57). The structure was refined successfully in $Pca2_1$, so *Pcam* was not considered.[29] After merging of the redundant data ($R_{merge} = 2.33\%$), 3558 reflections remained. The data/parameter ratio was 15.0 (3558 independent reflections and 237 parameters). All the data were included in the full-matrix least-squares refinement on F^2. The agreement factors were $wR_2 = 7.2\%$, R_1(all data) = 4.2%, $R_1(F_o > 4\sigma) = 3.2\%$, and GOF = 1.33.

The vanadium atoms show no statistically significant deviation from full occupancy. The largest peak in the difference Fourier map is less than 0.9 electron/Å^3, well into the noise level. Furthermore, no fractional occupancy atoms could be refined at the positions corresponding to reflection of the vanadium sites across the octahedral basal plane, where disorder had been found previously.[30]

The Flack parameter, refined in the initial stages of refinement, suggested the presence of racemic twinning. An inversion twin

(22) Beltrán-Porter, D.; Amorós, P.; Ibáñez, R.; Martínez, E.; Beltrán-Porter, A.; LeBail, A.; Ferey, G.; Villeneuve, G. *Solid State Ionics* **1989**, *32−33*, 57.
(23) Palkina, K. K.; Maksimova, S. I.; Chibiskova, N. T.; Schlesinger, K.; Ladwig, G. *Z. Anorg. Allg. Chem.* **1985**, *529*, 89.
(24) Murashova, E. V.; Chudinova, N. N. *Kristallografiya (Engl. Transl.)* **1994**, *39*, 129.
(25) Linde, S. A.; Gorbunova, Y. E.; Lavrov, A. V.; Kuznetsov, V. G. *Dokl. Akad. Nauk SSSR* **1979**, *244*, 1411.
(26) Hill, W. L.; Faust, G. T.; Hendricks, S. B. *J. Am. Chem. Soc.* **1943**, *65*, 794.
(27) Room-temperature single-crystal structure information for VPO: Enraf-Nonius CAD4 diffractometer; graphite monochromator, Mo Kα radiation, $\lambda = 0.710\,69$ Å; pure ω scans, $4.26 < 2\theta < 59.9°$; 6931 reflections (+ + +, + − +, + + −, + − −). Transmission factors ranged from 0.61 to 0.89. Absorption correction was based on ψ scans.
(28) The unit cell data were refined from the positions of 100 reflections (25 reflections, their negative-θ equivalents, and the Friedel pairs of those) in the range $16.76° < 2\theta < 31.14°$.
(29) The crystal structure was refined using SHELXL-97 (Sheldrick, 1997). All atoms were refined with anisotropic thermal parameters.

Table 1. Atomic Coordinates ($\times 10^4$) and Equivalent Isotropic Displacement Parameters ($Å^2 \times 10^3$) for $(VO)_2P_2O_7$ at 293 K

atom	*x*	*y*	*z*	*U*(eq)[a]
V(1)	7963(1)	9907(1)	1790(1)	7(1)
V(2)	7080(1)	10022(1)	3691(1)	6(1)
V(3)	2063(1)	5006(1)	4296(1)	6(1)
V(4)	2079(1)	5019(1)	1187(1)	6(1)
P(1)	6899(2)	2058(2)	5197(1)	5(1)
P(2)	2980(2)	2090(1)	5181(1)	6(1)
P(3)	2958(2)	7077(1)	2746(1)	6(1)
P(4)	6963(2)	7015(1)	2746(1)	6(1)
O(1)	4986(6)	10393(3)	1826(2)	12(1)
O(2)	5006(8)	10310(3)	3640(2)	12(1)
O(3)	27(8)	4865(4)	4329(2)	11(1)
O(4)	5003(6)	5106(3)	1152(2)	12(1)
O(5)	4953(5)	6740(3)	2761(3)	20(1)
O(6)	4958(5)	2127(3)	4912(2)	12(1)
O(7)	2783(7)	8698(4)	2731(2)	9(1)
O(8)	7229(6)	8624(4)	2748(2)	8(1)
O(9)	2492(7)	3658(4)	5241(2)	5(1)
O(10)	7484(8)	3612(4)	5247(2)	12(1)
O(11)	7027(5)	1410(4)	6003(3)	14(1)
O(12)	2904(5)	1391(4)	5997(2)	11(1)
O(13)	7824(5)	1315(4)	4539(3)	9(1)
O(14)	1960(5)	1437(4)	4510(3)	11(1)
O(15)	7637(5)	6398(3)	1983(2)	11(1)
O(16)	2217(6)	6479(4)	1998(2)	17(1)
O(17)	7722(6)	6373(4)	3496(3)	13(1)
O(18)	2233(5)	6516(4)	3511(3)	11(1)

[a] *U*(eq) is defined as one-third of the trace of the orthogonalized $\mathbf{U}_{ij}$ tensor.

matrix ($\bar{1}00$; $0\bar{1}0$; $00\bar{1}$) was applied, and the final refined value of BASF was 0.42(4). Although this result may be due to a twinned crystal, another explanation is that the structure is centrosymmetrically biased. The heavy atoms are close to pseudomirror planes, diminishing the effects of anomalous dispersion on the Friedel pairs.

3. Geometrical Parameters Important for the Spin Exchange Interactions of the Ribbon Chains

The vanadium and basal oxygen atoms forming the ribbon chains of the VPO phase are shown in Figure 1, where the phosphorus and apical oxygen atoms are omitted for simplicity. The perspective views along the *b*-direction of the V1−V2 and V3−V4 ribbon chains are presented in Figure 2. The corresponding views of the ribbon chains of the VHP phase are shown in Figure 3. Several geometrical parameters of the ribbon chains (Table 2) are important for our discussion because the magnetic orbitals (Figure 4a) of the spin monomers, VO_5 square pyramids, are contained in the planes parallel to the basal planes. Each SSE interaction along the ribbon chain is determined by the overlap between the O 2p orbitals of the O···O contacts in the two SSE paths V−O···O−V (Figure 4b). The magnitude of this interaction should increase as the O···O distances are decreased, as the O_4 ring formed from the two O···O contact units becomes more planar, and as the basal planes of the two spin monomers become more parallel.

Figure 3b shows that the ribbon chains of the VHP phase are strongly sinusoidal because the basal plane of each VO_5 square pyramid is inclined to the chain direction by ~30°. In contrast, the ribbon chains of the VPO phase are nearly straight. As a consequence, the V−V distance of each V_2O_8 dimer is shorter in VHP than in VPO, and so is the V···V distance between adjacent V_2O_8 dimers (Table 2). Another crucial difference between the ribbon chains of VHP and VPO lies in the way the V atoms of each V_2O_8 dimer are located with respect to the basal planes; they reside on one side in VHP (Figure 3b) (i.e., the cis arrangement) but on opposite sides in VPO (Figure 2) (i.e., the trans arrangement). The above two geometrical features are critical in our discussion of the relative strengths of the SE and SSE interactions in the VHP phase (section 6). Other geometrical parameters of the ribbon chains of the VPO and VHP phases are listed in Table 2.

For the discussion of the SE and SSE interactions of the VPO phase, it is important to know how strongly each ribbon chain twists from the ideal ribbon structure. For this purpose, we calculate the O−O−O−O dihedral angles of the consecutive O_4 rings along the ribbon chains (Table 3). The ribbon chains are not much twisted in the HPO structure of the VPO phase and in the VHP phase. However, in the APO structures of VPO, the V3−V4 ribbon chains are slightly twisted and the V1−V2 ribbon chains are strongly twisted in the O_4 rings associated with the SSE interactions (Table 3).

4. Spin Dimer Analysis

Magnetic properties of an electron-localized system are described by a spin-Hamiltonian expressed as a sum of pairwise spin exchange interactions. The strengths of spin exchange interactions (i.e., spin exchange parameters *J*) can be determined from first-principles electronic structure calculations for the high- and low-spin states of spin dimers (i.e., structural units consisting of two spin sites).[31−33] Recently, Petit et al.[34] examined the spin exchange interactions of VPO in terms of density functional theory calculations. In this study the geometries of various spin dimers were constructed on the basis of the earlier crystal structure of VPO whose atomic coordinates have low accuracy. The spin exchange parameters *J* can also be determined from first-principles electronic band structure calculations for various ordered spin arrangements of a magnetic solid.[35] These quantitative approaches become impractical for magnetic solids with large and complex unit cell structures. In explaining the anisotropy of spin exchange interactions of magnetic solids, however, it is sufficient to estimate the relative magnitudes of their *J* values.[21,36−47] In general, a spin

(30) Ebner, J. R.; Thompson, M. R. In *Structure−Activity and Selectivity Relationships in Heterogeneous Catalysis*; Grasselli, R. K., Sleight, A. W., Eds.; Elsevier: Amsterdam, 1991; pp 31−42.
(31) Illas, F.; Moreira, I. de P. R.; de Graaf, C.; Barone, V. *Theor. Chem. Acc.* **2000**, *104*, 265 and references therein.
(32) Noodleman, L. *J. Chem. Phys.* **1981**, *74*, 5737.
(33) Dai, D.; Whangbo, M.-H. *J. Chem. Phys.* **2001**, *114*, 2887.
(34) Petit, S.; Borshch, S. A.; Robert, V. *J. Am. Chem. Soc.* **2002**, *124*, 1744.
(35) Derenzo, S. E.; Klitenberg, M. K.; Weber, M. J. *J. Chem. Phys.* **2000**, *112*, 2074 and the references therein.
(36) Kahn, O. *Molecular Magnetism*; VCH Publishers: Weinheim, Germany, 1993.
(37) Hay, P. J.; Thibeault, J. C.; Hoffmann, R. *J. Am. Chem. Soc.* **1975**, *97*, 4884.
(38) Lee. K.-S.; Koo, H.-J.; Whangbo, M.-H. *Inorg. Chem.* **1999**, *38*, 2199.
(39) Koo, H.-J.; Whangbo, M.-H. *Solid State Commun.* **1999**, *111*, 353.

Table 2. Geometrical Parameters (Å, deg) Associated with the Ribbon Chains of $(VO)_2P_2O_7$ and $VO(HPO_4)\cdot 0.5H_2O$

compd	chain	param			
VHP[a]	V1−V2	V1−V2	3.087		
		V2···V1	4.318		
		O43···O4	2.543		
		O42···O41	2.537		
		∠O4−V1−O41	89.2		
		∠O42−V2−O43	90.9		
		∠V1−O51−V2	97.2		
		∠V1−O5−V2	97.1		
VPO/HPO	V−V	V−V	3.213		
		V···V	5.225		
		O···O	2.523		
		∠O−V−O	89.9		
		∠V−O−V	101.7		
			Geupel et al.	Hiroi et al.	this work
VPO/APO	V3−V4	V3−V4	3.205	3.180	3.205
		V4···V3	5.155	5.176	5.155
		O15···O17	2.512	2.492	2.510
		O16···O18	2.511	2.456	2.510
		∠O17−V3−O18	92.2	91.8	91.8
		∠O15−V4−O16	91.3	91.1	91.2
		∠V3−O9−V4	102.1	100.4	102.0
		∠V3−O10−V4	101.1	102.5	101.1
VPO/APO	V1−V2	V1−V2	3.228	3.255	3.227
		V2···V1	5.139	5.176	5.140
		O11···O13	2.532	2.534	2.506
		O12···O14	2.542	2.558	2.572
		∠O11−V1−O12	91.4	91.2	91.3
		∠O13−V2−O14	87.6	88.0	88.1
		∠V1−O7−V2	102.1	99.9	102.4
		∠V1−O8−V2	102.0	104.1	102.6

[a] Based on the 143 K crystal structure of ref 5.

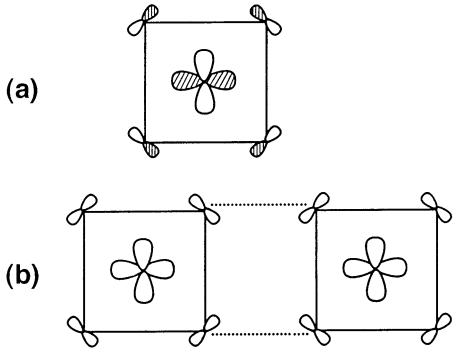

Figure 4. (a) Magnetic orbital of a VO_5 square pyramid, in which the V $3d_{xy}$ orbital is combined out-of-phase with the O 2p orbitals on the basal plane. (b) Overlap between two adjacent magnetic orbitals associated with the super-superexchange interaction along a ribbon chain. Since the V atom of a VO_5 square pyramid lies above the basal plane, the V $3d_{xy}$ orbital is not contained in the basal plane containing the O 2p orbitals.

exchange parameter J is written as $J = J_F + J_{AF}$, where the ferromagnetic term J_F (>0) is small so that the spin exchange becomes ferromagnetic (i.e., $J > 0$) when the antiferromagnetic term J_{AF} (<0) is negligibly small in magnitude. Thus antiferromagnetic spin exchange interactions (i.e., $J < 0$) can be discussed by focusing on the antiferromagnetic terms J_{AF}.[21,36−47]

Consider a spin dimer in which each spin site contains one unpaired electron and the two spin sites are equivalent

Table 3. O−O−O−O Dihedral Angles of the Consecutive O_4 Rings along the Ribbon Chains of $(VO)_2P_2O_7$ and $VO(HPO_4)\cdot 0.5H_2O$

compd	chain	ref	dihedral angles (deg)
VPO/APO	V3−V4[a]	Geupel et al.	(−7.7) (−7.5) (**0.7**) (7.7) (7.5) (**−0.7**)
		Hiroi et al.	(−7.1) (−7.2) (**0.7**) (7.1) (7.2) (**−0.7**)
		this work	(−7.7) (−6.8) (**−1.1**) (7.7) (6.8) (**1.1**)
VPO/APO	V1−V2[b]	Geupel et al.	(4.9) (−4.2) (**28.4**) (−4.9) (4.2) (**−28.4**)
		Hiroi et al.	(2.6) (−2.1) (**24.6**) (−2.6) (2.1) (**−24.6**)
		this work	(4.7) (−4.8) (**27.0**) (−4.7) (4.8) (**−27.0**)
VPO/HPO	V−V[c]	Azuma et al.	(−1.5) (1.5) (**0.0**) (−1.5) (1.5) (**0.0**)
VHP[d]	V1−V2[e]	Torardi and Calabrese	(−3.3) (−3.1) (**7.2**) (−3.3) (−3.1) (**7.2**)

[a] The sequence of the O−O−O−O dihedral angles along the V3−V4 ribbon chain is defined as (17−18−10−9), (9−10−16−15), (**15−16−18−17**), (17−18−10−9), (9−10−16−15), and (**15−16−18−17**), where the numbers in the parentheses refer to the oxygen numbers of Figure 1 and the dihedral angles associated with the super-superexchange paths are indicated by bold letters. [b] The sequence of the O−O−O−O dihedral angles along the V1−V2 ribbon chain is defined as (11−12−8−7), (7−8−14−13), (**13−14−12−11**), (11−12−8−7), (7−8−14−13), and (**13−14−12−11**), where the numbers in the parentheses refer to the oxygen numbers of Figure 1. [c] The sequence of the O−O−O−O dihedral angles along the V−V ribbon chains follows the same convention as defined above. [d] Based on the 143 K crystal structure of ref 5. [e] The sequence of the O−O−O−O dihedral angles along the ribbon chain is defined as (4−41−5−51), (51−5−42−43), (**43−42−41−4**), (4−41−5−51), (51−5−42−43), and (**43−42−41−4**), where numbers in the parentheses refer to the oxygen numbers of Figure 3.

(40) Whangbo, M.-H.; Koo, H.-J.; Lee, K.-S. *Solid State Commun*. **2000**, *114*, 27.
(41) Koo, H.-J.; Whangbo, M.-H. *J. Solid State Chem*. **2000**, *151*, 96.
(42) Koo, H.-J.; Whangbo, M.-H. *J. Solid State Chem*. **2000**, *153*, 263.
(43) Koo, H.-J.; Whangbo, M.-H. *Inorg. Chem*. **2001**, *40*, 2169.
(44) Koo, H.-J.; Whangbo, M.-H.; Coste, S.; Jobic, S. *J. Solid State Chem*. **2001**, *156*, 464.
(45) Dai, D.; Koo, H.-J.; Whangbo, M.-H. In *Solid State Chemistry of Inorganic Materials III*; MRS Symposium Proceedings Vol. 658; Geselbracht, M. J., Greedan, J. E., Johnson, D. C., Subramanian, M. A., Eds.; Materials Research Society: Warrendale, PA, 2001; pp GG5.3.1−5.3.11.
(46) Whangbo, M.-H.; Koo, H.-J.; Dai, D.; Villesuzanne, A. *J. Solid State Chem*. **2002**, *165*, 345.
(47) Koo, H.-J.; Whangbo, M.-H.; Dumas, J.; Continentino, M. A. *Inorg. Chem*. **2002**, *41*, 2193.

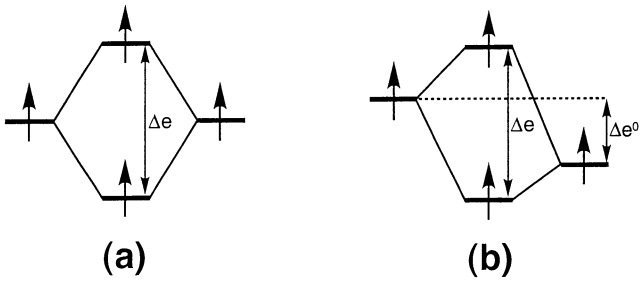

Figure 5. Orbital interaction between (a) equivalent and (b) nonequivalent spin sites of a spin dimer. The spin−orbital interaction energy $\Delta\epsilon$ is defined as $\Delta\epsilon = \sqrt{(\Delta e)^2-(\Delta e^0)^2}$, where $\Delta e^0 = 0$ for the case in (a).

and represented by nonorthogonal magnetic orbitals (i.e., singly occupied molecular orbitals of the spin monomers) ϕ_1 and ϕ_2. Provided that S and Δe are respectively the overlap integral and the spin−orbital interaction energy (Figure 5a) between ϕ_1 and ϕ_2, then the antiferromagnetic term J_{AF} varies as $J_{AF} \propto -(\Delta e)^2 \propto -S^2$.[36,37] In the case when the two spin sites of a spin dimer are nonequivalent (Figure 5b), the two magnetic orbitals differ in energy by Δe^0. For qualitative purposes, the extent of the antiferromagnetic spin exchange interaction can be discussed in terms of the net spin−orbital interaction energy, $\Delta e - \Delta e^0$. For semiquantitative purposes, however, it is necessary to employ the spin−orbital interaction $\Delta\epsilon = \sqrt{(\Delta e)^2-(\Delta e^0)^2}$.[36] The Δe^0 value can be estimated from the energies of the magnetic orbitals calculated for the spin monomers representing the two spin sites. Obviously, $\Delta e^0 = 0$, when the two spin sites are equivalent. For the simplicity of our notation, we will use the symbol $\Delta\epsilon$ to represent Δe for the case of two equivalent spin sites and $\sqrt{(\Delta e)^2-(\Delta e^0)^2}$ for the case of two nonequivalent spin sites.

Since J_{AF} is proportional to $-(\Delta\epsilon)^2$, it can be written as $J_{AF} = -\gamma(\Delta\epsilon)^2$. For antiferromagnetic spin exchange interactions, the proportionality constant γ can be estimated by comparing the calculated $(\Delta\epsilon)^2$ values with the corresponding J values determined experimentally. The spin−orbital interaction energy $\Delta\epsilon$ is approximately twice the hopping integral t (i.e., the resonance integral between ϕ_1 and ϕ_2), i.e., $\Delta\epsilon \approx 2t$. From the relationship[36,37,48−50]

$$J_{AF} = -4t^2/U_{eff} \approx -(\Delta\epsilon)^2/U_{eff}$$

we obtain $\gamma \approx 1/U_{eff}$, where U_{eff} is the effective on-site repulsion. For a set of closely related magnetic solids, the U_{eff} value would be nearly constant and hence could be used to approximate antiferromagnetic J by $-(\Delta\epsilon)^2/U_{eff}$.

In reproducing the trends in spin exchange interactions of magnetic solids using $\Delta\epsilon$ values obtained from extended Hückel calculations,[51,52] it is found necessary to employ double-ζ Slater type orbitals (DZ STO's) for both the 3d orbitals of the transition metal and the s/p orbitals of the surrounding ligand atoms.[21,38−47,49,50] The atomic orbital parameters of V and O employed for our extended Hückel tight-binding calculations are listed in Table 4. The radial part of the O 2p orbital, $\chi_{2p}(r)$, is written as

$$\chi_{2p}(r) = r[C \exp(-\zeta r) + C' \exp(-\zeta' r)]$$

where the exponents ζ and ζ' describe contracted and diffuse STO's, respectively (i.e., $\zeta > \zeta'$). The diffuse STO provides an orbital tail that enhances overlap between O atoms in the short O···O contacts of the V−O···O−V super-superexchange paths as well as that between the V 3d and O 2p orbitals of the V−O−V super-exchange paths. The $\Delta\epsilon$ values are affected most sensitively by the exponent ζ' of the diffuse STO of the O 2p orbital. To determine the appropriate ζ' value, we carry out spin dimer analysis as a function of ζ' by gradually increasing it as $\zeta'(x) = 1.659(1 + x)$ from the value 1.659 taken from the atomic orbital calculations.[53] Earlier studies on the magnetic solids Cu_4O_3 and $Ag_2Cu_2O_3$ show that the x value appropriate for spin exchange interactions of magnetic oxides is in the range of 0.10−0.13.[49]

Table 4. Exponents ζ_i and Valence Shell Ionization Potentials H_{ii} of Slater-Type Orbitals χ_i Used for Extended Hückel Tight-Binding Calculation[a]

atom	χ_i	H_{ii} (eV)	ζ_i	C[b]	ζ_i'	C'[b]
V	4s	−8.81	1.697	1.0		
V	4p	−5.52	1.260	1.0		
V	3d	−11.0	5.052	0.3738	2.173	0.7456
O	2s	−32.3	2.88	0.7076	1.675	0.3745
O	2p	−14.8	3.694	0.3322	1.659	0.7448

[a] H_{ii}'s are the diagonal matrix elements $\langle\chi_i|H^{eff}|\chi_i\rangle$, where H^{eff} is the effective Hamiltonian. In our calculations of the off-diagonal matrix elements $H^{eff} = \langle\chi_i|H^{eff}|\chi_j\rangle$, the weighted formula was used. See: Ammeter, J.; Bürgi, H.-B.; Thibeault, J. C.; Hoffmann, R. *J. Am. Chem. Soc.* **1978**, *100*, 3686. [b] Contraction coefficients used in the double-ζ Slater-type orbital.

5. Spin Exchange Interactions of the VPO Phase

How different the V1 and V2 atoms are in the V1−V2 ribbon chain can be seen by calculating the energy difference Δe^0 between the spin monomers $V1O_5$ and $V2O_5$. Likewise, how different the V3 and V4 atoms are in the V3−V4 ribbon chain can be measured by calculating the energy difference Δe^0 between the spin monomers $V3O_5$ and $V4O_5$. Figure 6 shows the Δe^0 values calculated for the three APO structures of VPO as a function of the O 2p exponent $\zeta'(x)$. In Geupel et al.'s[11] structure, the V1 and V2 environments are slightly different, and so are the V3 and V4 environments. In our structure, the difference between V3 and V4 is smaller than that of Geupel et al.'s whereas that between V1 and V2 is somewhat larger than that of Geupel et al.'s. In Hiroi et al.'s[10] structure, the V3 and V4 atoms are strongly different.

Figure 7a−d shows the spin−orbital interaction energies $\Delta\epsilon$ calculated for the HPO and APO structures of VPO as a function of the exponent $\zeta'(x)$. The SSE and SE interactions of the V1−V2 and V3−V4 ribbon chains determined from Geupel et al.'s structure (Figure 7b) are quite similar to those

(48) This expression is valid when spin exchange parameters of a spin Hamiltonian are written as J instead of $2J$.
(49) Whangbo, M.-H.; Koo, H.-J. *Inorg. Chem.* **2002**, *41*, 3570.
(50) Whangbo, M.-H.; Koo, H.-J.; Lee, K.-S. *J. Solid State Chem.*, in press.
(51) Hoffmann, R. *J. Chem. Phys.* **1963**, *39*, 1397.
(52) Our calculations were carried out by employing the *CAESAR* program package (Ren, J.; Liang, W.; Whangbo, M.-H. *Crystal and Electronic Structure Analysis Using CAESAR*; 1998; http://www. PrimeC.com/).
(53) Clementi, E.; Roetti, C. *At. Data Nucl. Data Tables* **1974**, *14*, 177.

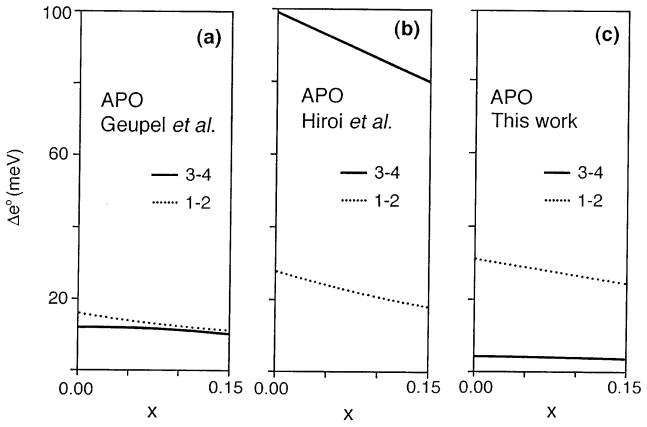

Figure 6. Δe^0 values associated with the two nonequivalent spin monomers in the V3−V4 and V1−V2 ribbon chains of $(VO)_2P_2O_7$ calculated for the APO structure of (a) Geupel et al.,[11] (b) Hiroi et al.,[10] and (c) this work as a function of the exponent $\zeta'(x)$ of the O 2p orbital. The V3−V4 and V1−V2 ribbon chains are referred to as 3−4 and 1−2, respectively.

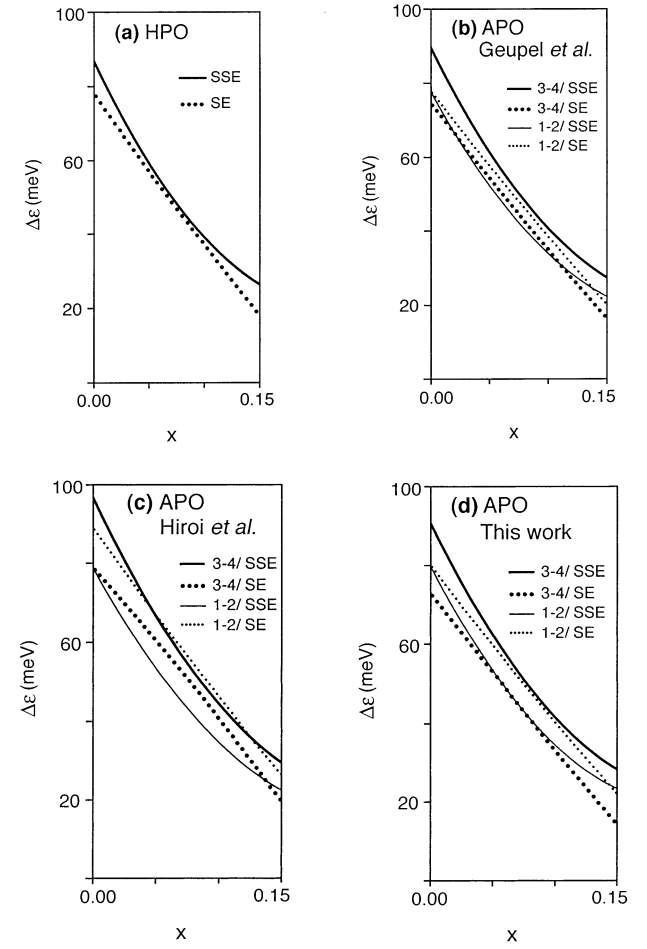

Figure 7. Spin−orbital interaction energies $\Delta\epsilon$ of the superexchange and super-superexchange interactions in the ribbon chains of $(VO)_2P_2O_7$ calculated for the HPO structure of (a) Azuma et al.[17] and for the APO structure of (b) Geupel et al.,[11] (c) Hiroi et al.,[10] and (d) this work as a function of the exponent $\zeta'(x)$ of the O 2p orbital. In (b)−(d), the V3−V4 and V1−V2 ribbon chains are referred to as 3−4 and 1−2, respectively.

determined from our structure (Figure 7d). In contrast, Hiroi et al.'s structure provides a quite different picture (Figure 7c), due in large part to the fact that the local environments of the V3 and V4 atoms are strongly different in their

Table 5. Comparison of the $\Delta\epsilon$ (meV) and J/k_B (K) Values Calculated for the Superexchange and Super-superexchange Interactions in the V3−V4 and V1−V2 Ribbon Chains of the Ambient-Pressure Structures of $(VO)_2P_2O_7$[a,b]

chain	spin exchange		$\Delta\epsilon$	$-J/k_B$[a]
V3−V4	SSE	Geupel et al.	41	130
		Hiroi et al.	45	156
		this work	42	136 (136,[c] 135 ± 5[d])
V3−V4	SE	Geupel et al.	35	94
		Hiroi et al.	44	149
		this work	33	84 (92,[c] 115 ± 6[d])
V1−V2	SSE	Geupel et al.	34	89
		Hiroi et al.	35	94
		this work	35	94 (103,[c] 81 ± 3[d])
V1−V2	SE	Geupel et al.	38	111
		Hiroi et al.	46	163
		this work	40	123 (124,[c] 127 ± 3[d])

[a] The calculated J values were obtained from the expression $J = -(\Delta\epsilon)^2/U_{eff}$ with $U_{eff} = 151$ meV. [b] The experimental $-J/k_B$ values listed in parentheses are arranged such that the largest experimental $-J/k_B$ value agrees with the largest calculated $-J/k_B$ value. [c] Neutron scattering measurements (taken from ref 15). [d] Magnetic susceptibility measurements (taken from ref 17).

structure. In the HPO structure,[18,19] the SSE interaction is stronger than the SE interaction for all x values (Figure 7a). The spin exchange parameters deduced experimentally for the HPO structure are $J_1/k_B = -131.6$ K and $J_2/k_B = -114.6$ K[17] so that J_1 should be assigned to the SSE interaction and J_2 to the SE interaction. The experimental J_1/J_2 ratio of 1.15 is well approximated by the corresponding $(\Delta\epsilon_1/\Delta\epsilon_2)^2$ value when $x = 0.10$. Figure 7a shows that another value of x smaller than 0.10 (i.e., 0.05) can also reproduce the same result. However, we choose $x = 0.10$ because the earlier study of other magnetic oxides shows that the appropriate range for x is 0.10−0.13.[49] Thus, we employ the $\Delta\epsilon$ values calculated with $x = 0.10$ to evaluate $J_{AF} = -(\Delta\epsilon)^2/U_{eff}$ for the APO structures. These $\Delta\epsilon$ values are summarized in Table 5.

The J/k_B value of the strongest antiferromagnetic interaction deduced experimentally for the APO structure is −136 K.[15] This J is reproduced by $J_{AF} = -(\Delta\epsilon)^2/U_{eff}$ on the basis of the $\Delta\epsilon$ value calculated from our crystal structure if the U_{eff} value is taken as 151 meV. Using this U_{eff} we calculate the J values expected for the SSE and SE interactions on the basis of the calculated $\Delta\epsilon$ values (Table 5). The J values calculated from Hiroi et al.'s structure differ significantly from the experimental values. In contrast, the J/k_B values estimated from Geupel et al.'s and our structures are very close. Table 5 summarizes the calculated J/k_B values as well as the experimental J/k_B values deduced from the neutron scattering[15] and the magnetic susceptibility[17] measurements. For the spin exchange interactions of the APO structure our calculations based on the accurate crystal structures led to the following conclusions:

(a) The ribbon chain with the larger spin gap (i.e., the larger difference in the J/k_B values) is the V3−V4 ribbon chain, and that with the smaller spin gap (i.e., the smaller difference in the J/k_B values) is the V1−V2 ribbon chain.

(b) The SSE interaction is stronger than the SE interaction in the larger spin-gap ribbon chain, while the opposite is the case in the smaller spin-gap ribbon chain.

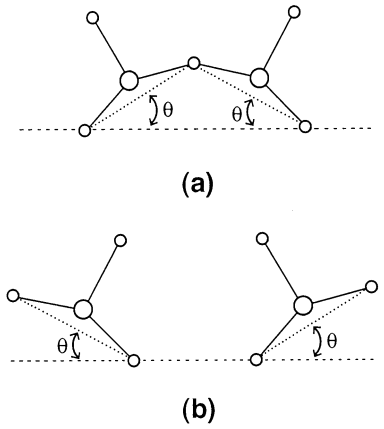

Figure 8. Spin dimers describing the (a) superexchange and (b) super-superexchange interactions in the ribbon chains of $VO(HPO_4)\cdot 0.5H_2O$. The basal plane of each VO_5 square pyramid is inclined to the chain direction by the angle θ, and the geometries of the spin dimers are assumed to possess a C_{2v} symmetry.

(c) The above observations are consistent with the experimental $-J/k_B$ values derived from the neutron scattering measurements[15] but not with those derived from the magnetic susceptibility measurements.[17]

The SSE interaction is much stronger in the V3−V4 chain than in the V1−V2 chain, because the O_4 ring associated with the SSE paths is almost planar in the V3−V4 ribbon chain but is strongly twisted in the V1−V2 ribbon chain (Table 3). The earlier studies[10,16] assigned the larger spin gap to the V1−V2 chain assuming that in a given type of spin exchange interaction the magnitude of the interaction decreases with increasing the V−V distance. This assumption is not supported because the strength of an antiferromagnetic spin exchange interaction is determined mainly by the p-orbital tails of magnetic orbitals and hence can be strongly affected by a geometrical parameter other than the metal−metal distance.

6. Spin Exchange Interactions of the VHP Phase

The room-temperature and 143 K crystal structure[5] data for VHP employed for our spin dimer analysis are given in the Supporting Information. The two structures are quite similar, except that two slightly different V atoms are present in the low-temperature structure while all V atoms are equivalent in the room-temperature structure. In the VHP phase the basal planes of the VO_5 square pyramids are inclined to the ribbon-chain direction by ∼30° (Figure 3b). To examine the effect of the inclination angle θ on the spin exchange interactions, we calculate the spin−orbital interaction energies for the SE and SSE interactions (hereafter referred to as $\Delta\epsilon_1$ and $\Delta\epsilon_2$, respectively) as θ is gradually increased from 0 to 30° (Figure 8). For these model calculations, the geometries of the spin dimers representing the SE and SSE interactions were idealized to have a C_{2v} symmetry by employing the average V−O bond lengths and average −O−V−O bond angles on the basis of the 143 K structure. Our results are summarized in Figure 9a. Though not shown, our spin dimer analyses carried out for the room-temperature crystal structure of VHP[5] and for the room-temperature and 10 K crystal structures of VDP[20,54] led to the same results as described below.

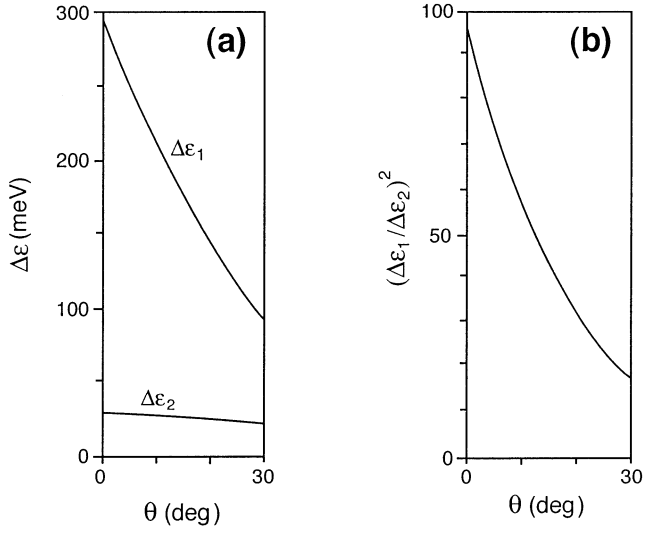

Figure 9. Dependence of the spin exchange interactions of $VO(HPO_4)\cdot 0.5H_2O$ on the inclination angle θ calculated by using the O 2p orbital $\zeta'(x)$ value for $x = 0.10$: (a) spin−orbital interaction energies of the superexchange ($\Delta\epsilon_1$) and super-superexchange ($\Delta\epsilon_2$) interactions; (b) $(\Delta\epsilon_1/\Delta\epsilon_2)^2$.

The $\Delta\epsilon_1$ and $\Delta\epsilon_2$ values important for the SE and SSE interactions of VHP are those in the vicinity of 30°. Let us first consider these values around $\theta \approx 30°$. Figure 9a shows that the SE interaction is much stronger than the SSE interaction around $\theta \approx 30°$. This is understandable because the overlap between the two magnetic orbitals associated with the SSE interaction (Figure 4b) is reduced at the large inclination angle. The inclination of the basal plane also reduces the SE interaction, but the reduction of the SE interaction is considerably weaker than that of the SSE interaction because the overlap between the V $3d_{xy}$ and the O 2p orbitals in the SE paths V−O−V is not strongly reduced by the inclination. We now examine the dependence of the $\Delta\epsilon_1$ and $\Delta\epsilon_2$ values on the inclination angle. As θ decreases from 30°, the $\Delta\epsilon_2$ for the SSE interaction increases as expected, but the $\Delta\epsilon_1$ of the SE interaction increases much more sharply. The latter is caused by the fact that the V atoms of a V_2O_8 dimer have the cis arrangement so that as θ approaches 0°, the V $3d_{xy}$ orbitals of the V_2O_8 dimer become more coplanar hence greatly enhancing their direct overlap. The ratio of the spin exchange parameter of the SE interaction to that of the SSE interaction is approximated by $(\Delta\epsilon_1/\Delta\epsilon_2)^2$. As shown in Figure 9b, the $(\Delta\epsilon_1/\Delta\epsilon_2)^2$ value is ∼20 at $\theta \approx 30°$. This explains why the spin exchange interactions of VHP and VDP are well described by the isolated dimer model.[8,20]

In the vicinity of $\theta \approx 0°$, the spin−orbital interaction energy for the SE interaction of the VHP phase is stronger than those of the VPO phase by a factor of 7−8 (Table 5 and Figure 9a). This is due to the fact that the V atoms of a V_2O_8 dimer have the cis arrangement in VHP but the trans arrangement in VPO. The effect of the direct overlap between

(54) Garrett, A. W. Ph.D. Thesis, University of Florida, 1988.

the V $3d_{xy}$ orbitals is strongly reduced in the SE interaction of VPO, because they are not coplanar unlike the case of the SE interaction in VHP. This observation reinforces our conclusion that the SE interaction should dominate over the SSE interaction in the ribbon chains of VHP. Thus, the isolated spin dimers of VHP are formed by the SE interactions and not by the SSE interactions. This is in disagreement with the conclusion deduced from the neutron scattering study using powder samples of VDP.[20] As described above, however, it is compelling from geometrical and electronic reasons that the SE interaction must dominate over the SSE interaction in VHP. In addition, the present method of spin dimer analysis has been successful in describing the trends in spin exchange interactions for a variety of other magnetic solids.[38−47,49,50] Thus, it is difficult to imagine that this method would fail selectively for VHP. Obviously, our dilemma is that from the perspective of interpreting the powder neutron scattering data,[20] which involves powder averaging over the neutron scattering structure factor of a dimer and hence requires the absence of any preferred orientation in powder samples, it is unavoidable to arrive at the opposite conclusion.

7. Concluding Remarks

As evidenced by the present single-crystal X-ray structure determination, high-quality single-crystal samples of VPO can be grown from a phosphorus pentoxide flux. The spin dimer analysis based on the two high-precision crystal structures of VPO, Geupel et al.'s[11] and ours, shows unambiguously that the V3−V4 chain has a larger spin gap than does the V1−V2 chain and that the SSE interaction is stronger than the SE interaction in the V3−V4 chain while the opposite is true in the V1−V2 chain. Both structural and electronic reasons show that the isolated spin dimers of VHP are formed by the SE interactions, not by the SSE interactions, in disagreement with the conclusion of the powder neutron scattering study.[20] To resolve these irreconcilable conclusions, further studies are necessary.

Acknowledgment. The authors wish to thank P. Kelly and M. Plummer for technical assistance and H. S. Horowitz and J. C. Calabrese for helpful discussions. M.-H.W. wishes to thank S. E. Nagler for making available the crystal structures of $VO(DPO_4)\cdot 0.5D_2O$. The work at North Carolina State University was supported by the Office of Basic Energy Sciences, Division of Materials Sciences, U.S. Department of Energy, under Grant DE-FG02-86ER45259.

Supporting Information Available: Crystallographic data and anisotropic thermal parameters of $(VO)_2P_2O_7$ at room temperature (Tables S1 and S2) and crystallographic data, positional parameters, and anisotropic thermal parameters of $VO(HPO_4)\cdot 0.5H_2O$ at room temperature (Tables S3−S5) and at 143 K (Tables S6−S8). This material is available free of charge via the Internet at http://pubs.acs.org.

IC020249C